

Decomposition of entropy production for free-energy generation in a non-equilibrium dot with multiple electron states

Chloe Salhani, Kensaku Chida, Takase Shimizu, Toshiaki Hayashi, and Katsuhiko Nishiguchi*
NTT Basic Research Laboratories, Nippon Telegraph and Telephone Corporation, Kanagawa, Japan

(Dated: January 29, 2025)

We experimentally demonstrate the decomposition of entropy production during free-energy generation in a nanometer-scale dot transitioning to a non-equilibrium steady state via single-electron counting statistics. An alternating-current signal driving a reservoir that injects multiple electrons into the dot makes it non-equilibrium, leading to free-energy generation, heat dissipation, and Shannon-entropy production. By analyzing the time-domain probability distributions of multiple electron states of the dot, we quantitatively decompose the heat dissipation into housekeeping and excess heats, revealing the correlation between the free energy and the decomposed components of heat dissipation. This correlation suggests that the ratio of the generated free energy to the work applied to the dot, can potentially reach 0.5 under far-from-equilibrium conditions induced by a large signal, while an efficiency of 0.25 was experimentally achieved. Our results, providing the theoretical and experimental efficiencies from the relation between decomposed heat dissipation and free-energy generation, promise to connect non-equilibrium thermodynamics perspectives to electronic devices.

Thermodynamics provides information on theoretical performance limits of systems, such as the energy cost of information processing, known as the Landauer limit [1]. Some experiments using microscopic systems have successfully demonstrated these theories [2–8]. However, theories and experiments both rely on quasi-static operations near equilibrium. In contrast, real-world applications often require non-equilibrium conditions to achieve practical performance, including speed, power, and efficiency.[9–12]

A non-equilibrium state is induced when an external force drives a system out of the global detailed balance, causing entropy production. This entropy production or its rate $\dot{\sigma}$ can be decomposed into two components representing the state transition [13–16]. (Throughout this paper, the dot notation $\dot{\square}$ represents the time derivative of \square .) The first component is the excess or nonadiabatic entropy production $\dot{\sigma}_{\text{EX}}$, and the second is the housekeeping or adiabatic entropy production $\dot{\sigma}_{\text{HK}}$. This decomposition provides non-equilibrium thermodynamics perspectives such as the non-negativity and fluctuation theory of $\dot{\sigma}_{\text{EX}}$ and $\dot{\sigma}_{\text{HK}}$ [14, 15, 17–21], which would offer critical constraints for electronic applications close to thermal fluctuation for low energy consumption. [22–26]

The qualitative natures of $\dot{\sigma}_{\text{EX}}$ and $\dot{\sigma}_{\text{HK}}$ are expected to offer other crucial insights into electronic device performance. $\dot{\sigma}_{\text{EX}}$ reflects energy consumed during signal transitions, while $\dot{\sigma}_{\text{HK}}$ represents the energy consumed to maintain the signals. Since electronic devices operate dynamically with these input and output signals, understanding and connecting $\dot{\sigma}_{\text{EX}}$ and $\dot{\sigma}_{\text{HK}}$ to electronic engineering parameters is crucial for minimizing energy consumption in devices. Several theoretical stud-

ies have analyzed entropy production in devices, including diodes and transistors, from the stochastic thermodynamics perspective. [10, 27–29] Experimental quantification of entropy production have also been achieved by analyzing single-electron motion in single-electron devices. [4, 8, 30–35] However, to the best of our knowledge, no experimental decomposition of entropy production into $\dot{\sigma}_{\text{EX}}$ and $\dot{\sigma}_{\text{HK}}$ has been reported.

Free energy generated by external forces is also crucial in thermodynamics and device operation. While large free energy is generally desired, its acquisition inevitably leads to entropy production. $\dot{\sigma}_{\text{EX}}$, related to how far the system is from the steady state, is expected to correlate with free energy. The relationship between $\dot{\sigma}_{\text{HK}}$ and free energy is less clear, but minimizing $\dot{\sigma}_{\text{HK}}$ is generally understood to reduce the overall cost of free energy acquisition. Therefore, understanding these correlations is essential for operating systems with high free energy and low cost, i.e., high efficiency.

The number of electrons used in devices is a factor requiring careful discussion. In previous studies,[4, 8, 30–35] the presence and absence of a single electron in a small dot have been analyzed under the condition that the charging energy of the dot is larger than the thermal energy. Such a condition generates a unique dependence of statistical parameters governing thermally agitated electron motion, i.e., thermal noise, on the charging energy and charge offset within the dot, unlike the multiple-electron case, as demonstrated in Ref. [36]. Although theoretical reports have analyzed multiple-electron motion through devices,[10, 27–29] there are few experimental reports.

In this study, we quantify and analyze decomposed entropy production and free energy in a non-equilibrium small dot with multiple electron states driven by an alternating-current (AC) signal. Employing single-

* katsuhiko.nishiguchi@ntt.com

electron counting statistics, we monitor the individual motions of multiple electrons within the dot constituting a device that mimics dynamic random access memory (DRAM), thereby revealing the correlation between heat dissipation, free-energy generation, and their efficiency. These thermodynamics insights gained from DRAM can be extended to other electronic components. This is because a capacitor, representing information, is a major passive component, alongside a resistor and because a DRAM combines a capacitor and a transistor functioning as a variable resistor. Therefore, employing a DRAM provides a valuable bridge between thermodynamics perspectives and electronic-device performance.

Figure 1(a) shows our device for single-electron counting statistics: the individual motion of single electrons traveling back and forth between an electron reservoir (ER) and the dot is monitored. Since all measurements were carried out at room temperature, the electron motion originates not from tunneling events but from thermal hopping over an energy barrier under a lower gate (LG) [see Fig. 1(b)]. [37] These structures and principles are similar to conventional DRAMs, except that the dot in our device is very small (about 10 attofarads in capacitance), storing approximately twenty electrons. The electrons in the dot are counted with a field-effect transistor (FET), referred to as the sense-FET: the current flowing through the sense-FET increases/decreases in a step-like pattern when a single electron leaves/enters the dot, as shown in Fig. 1(c). From the step height caused by a single electron and the sense-FET's transconductance, the charging energy E_C for one electron stored in the dot was estimated to be 9.8 meV. [38]

We control equilibrium and non-equilibrium states between the ER and the dot, hereafter defined as the ER-dot system, by modulating the Fermi energy of the ER. [39] In the equilibrium state, constant voltages are applied to the ER and LG, respectively. Since the energy barrier height controlled by the LG governs the transition rate of electrons surmounting the barrier considering Kramer's rate, [40] the transition rate Γ_0 for an electron to enter the dot is constant, while the rate Γ_N^- for an electron to leave the dot is given by $\Gamma_0 \exp(\beta\mu_N)$, where $\mu_N = 2E_C(N - 0.5)$ is the chemical potential of the dot, N is the deviation from the average number N_0 of electrons in the dot at equilibrium [see Fig. 1(b)], $\beta = (k_B T)^{-1}$ is the inverse temperature, k_B is the Boltzmann constant, and T is the temperature. These transition rates are estimated experimentally from the transient characteristics of N . [41] Γ_0 is adjusted to be 0.1 Hz to ensure the electron motion is slow enough to be precisely monitored.

The non-equilibrium state is induced by superimposing an AC voltage signal, $V(t) = S_{AC} \sin(\omega_{AC} t + \phi)$, on the constant ER voltage. [39] Here, S_{AC} , $\omega_{AC}/2\pi$, and ϕ are the amplitude, frequency, and phase of the AC signal. The period $2\pi/\omega_{AC}$ of the AC signal is significantly longer than the time required for an electron

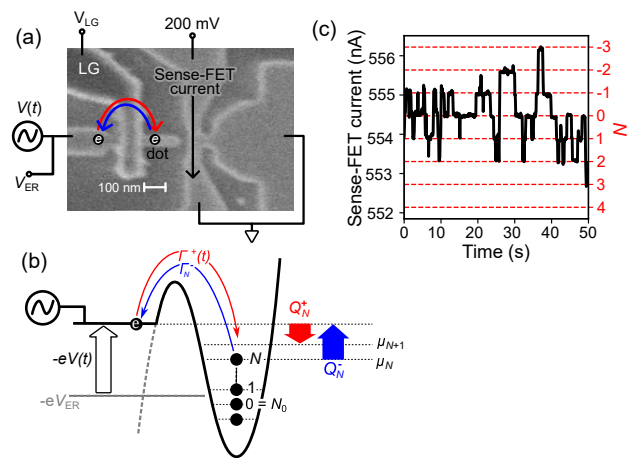


FIG. 1: (a) Scanning-electron-microscope (SEM) image of the device for single-electron counting statistics. The constant ER voltage V_{ER} was 0.5 V. The details of the device fabrication is explained in Appendix A and Ref. [38]. (b) Energy band diagram between the ER and dot. The Fermi energy of the ER is modulated by an AC signal $V(t)$ superimposed on V_{ER} . (c) Current flowing through the sense-FET without the AC signal. The sampling rate of the sense-FET was 20 Hz.

to travel between the ER and the dot and to dissipate its energy gained from the AC signal. Since electrons in the ER surmount the energy barrier whose height is changed by $-eV(t)$, the transition rate $\Gamma^+(t)$ for the electron to enter the dot is modulated over time, $\Gamma^+(t) = \Gamma_0 \exp[-\beta eV(t)]$. Since the transition rate to leave the dot remains independent of the AC signal, Γ_N^- given by $\Gamma_0 \exp(\beta\mu_N)$ still holds. In this report, $\omega_{AC}/2\pi$ of 1 Hz larger than Γ_0 prevents electrons from following the AC signal and thus pushes the ER-dot system out of equilibrium.

To perform a statistical analysis, we repeated measurements of the sense-FET current when the AC signal was applied with random ϕ , converted them into the change in N , and averaged them. In the theoretical analysis, we assume that ϕ and time-average $V(t)$ are zero.

Equilibrium and non-equilibrium states of the ER-dot system were studied via statistical analysis on the time-dependent probability $\rho_N(t)$ for the dot to contain the excess electron number N at time t . Figures 2(a) and (b) show the distributions of $\rho_N(t)$ over time t when an AC signal was applied at $t = 0$. To characterize equilibrium and non-equilibrium states of the ER-dot system, we consider the average $\langle N(t) \rangle$, given by $\sum_{N=-\infty}^{\infty} \rho_N(t) N$, and the variance $\sigma^2(t)$, given by $\sum_{N=-\infty}^{\infty} \rho_N(t) [N - \langle N(t) \rangle]^2$, of N at time t , which are summarized in Fig. 2(c).

Before the AC signal is applied, the system is in equilibrium: $\rho_N(t)$ follows a Gaussian distribution with a mean $\langle N(t) \rangle$ of zero and a variance $\sigma^2(t)$ given by $(2\beta E_C)^{-1}$ as shown by the $\rho_N(t_1)$ distribution in Fig. 2(b), meaning the electron motion between the ER and the dot is

thermally-activated.[41] After the AC signal is applied, the dynamic change in the ER voltage causes a temporal disruption of the detailed balance condition, placing the ER-dot system in non-equilibrium. The bell-shaped distribution of $\rho_N(t)$ shifts positively in N and $\langle N(t) \rangle$ increases over time. Meanwhile, $\sigma^2(t)$ initially increases, as shown by the $\rho_N(t_2)$ distribution, and then decreases. Finally, after $t \sim 1/\Gamma_0$, the $\rho_N(t)$ distribution stabilizes to a Gaussian distribution with a variance $\sigma^2(t)$ given by $(2\beta E_C)^{-1}$, as shown by the $\rho_N(t_3)$ distribution. In this case, the transition rate for electrons entering the dot balances with the rate of escaping electrons, meaning the local detailed balance holds between the ER and the dot, reaching a non-equilibrium steady state.[39]

The dynamics of the ER-dot system can be described by the following master equation:

$$\dot{\rho}_N(t) = \Gamma^+(t)\rho_{N-1}(t) - [\Gamma^+(t) + \Gamma_N^-]\rho_N(t) + \Gamma_{N+1}^-\rho_{N+1}(t), \quad (1)$$

where $\sum_{N=-\infty}^{\infty} \rho_N(t) = 1$. Since $\Gamma^+(t)$ is time-dependent, solving the set of equations is not always possible. To avoid this issue, we assume that $\Gamma^+(t)$ is replaced by its time average $\overline{\Gamma^+}$ given by the modified Bessel function $I_0(\beta e S_{AC})$ (also see Appendix D).[39] As shown in Fig. 2(c), the numerical results of the master equation trace the experimental results well, implying that $\overline{\Gamma^+}$ functions as the effective transition rate for an electron entering the dot.

Figures 2(a), (b), and (c) provide information on the free energy and Shannon entropy in the dot during the state transition. Since the contribution of the Shannon entropy to energy is small, as explained next, the generation $\Delta F(t)$ of free energy is defined by $E_C \langle N(t) \rangle^2$ [42]. It monotonically increases and then asymptotically reaches $E_C \langle N_{SS} \rangle^2$ after $t \sim 1/\Gamma_0$, as shown in Fig. 2(d), where $\langle N_{SS} \rangle$ given by $\ln(\overline{\Gamma^+}/\Gamma_0)/(2\beta E_C)$ is the average excess electron number in the non-equilibrium steady state.[39]

Shannon entropy $S(t)$ is given by $-\sum_{N=-\infty}^{\infty} \rho_N(t) \ln \rho_N(t)$, and its difference $\Delta S(t)$ from the initial equilibrium state is defined as $S(t) - S(0)$. During the state transition from the equilibrium state to the non-equilibrium steady state, $\sigma^2(t)$ increases, leading to an increase in $\Delta S(t)$. In the non-equilibrium steady state, $\sigma^2(t)$ returns to its initial value $(2\beta E_C)^{-1}$, as confirmed at various values of ω_{AC} and S_{AC} in Ref. [39], meaning $\Delta S(t) = 0$ in the steady state. Additionally, $\Delta S(t)$ is much smaller than $\Delta F(t)$ as shown in Fig. 2(d) as well as the heat dissipation explained in the next section. Therefore, we consider the entropy production to be dominated by heat dissipation.

The heat-dissipation rates for individual electron motion between the ER and the dot are derived from probability flows, given by $\rho_N(t)\Gamma^+(t)$ and $\rho_N(t)\Gamma_N^-$, and the heat dissipated by a single electron entering and leaving the dot (see Appendix B). The total heat dissipation rate \dot{Q}_T is defined as $\dot{Q}_T = \dot{Q}^+ + \dot{Q}^-$. Here, \dot{Q}^+ and \dot{Q}^- are the

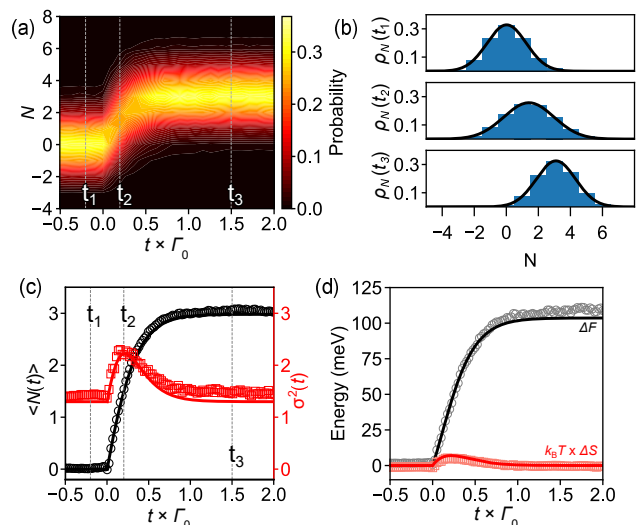


FIG. 2: (a) Contour plot of the $\rho_N(t)$ distributions from an equilibrium state to a non-equilibrium steady state. The AC signal with amplitude S_{AC} of 100 mV was applied at $t = 0$. Experimental data were averaged over 3000 repetitions. (b) $\rho_N(t)$ distributions at t_1 , t_2 , and t_3 depicted in (a). The solid lines are the Gaussian fits to the experimental results. (c) Transient characteristics of $\langle N(t) \rangle$ and $\sigma^2(t)$. (d) Transient characteristics of the free energy δF and $k_B T$ multiplied by the deviation ΔS of the Shannon entropy from its initial value at $t = 0$. In (c) and (d), open circles are the experimental data, and the solid lines are the numerical results of the master equation shown by Eq. (1).

heat dissipation rates for electrons entering and leaving the dot, respectively:

$$\dot{Q}^+ = \sum_{N=-\infty}^{\infty} \rho_N(t) \Gamma^+(t) [-eV(t) - \mu_{N+1}] \quad \text{and} \quad (2)$$

$$\dot{Q}^- = \sum_{n=-\infty}^{\infty} \rho_N(t) \Gamma_N^- [eV(t) + \mu_N], \quad (3)$$

from Eqs. (B2) and (B3) in Appendix B.

Next, we consider heat dissipation in a steady state. $\rho_N(t)$ in the steady state stabilizes to a Gaussian distribution: $\rho_N^{SS} = Z^{-1} \exp[-\beta E_C (N - \langle N_{SS} \rangle)^2]$, where $Z = \sum_{N=-\infty}^{\infty} \rho_N^{SS}$ [see Appendix B]. Given that μ_N , ρ_N^{SS} , μ_N , and Γ_N^- are time-independent, that $\Gamma^+(t)$ is averaged over time, i.e., $\overline{\Gamma^+}$, and that the phase or time-averaged $V(t)$ is zero, Eqs. (2) and Eq. (3) yield \dot{Q}^+ and \dot{Q}^- in a steady state:

$$\dot{Q}^{+SS} = -eV(t) \Gamma^+(t) - 2E_C (\langle N_{SS} \rangle + 0.5) \overline{\Gamma^+} \quad \text{and} \quad (4)$$

$$\dot{Q}^{-SS} = 2E_C (\langle N_{SS} \rangle + 0.5) \overline{\Gamma^+} \quad (5)$$

Consequently, \dot{Q}_T in a steady state becomes

$$\dot{Q}_T^{SS} = \dot{Q}^{+SS} + \dot{Q}^{-SS} = -eV(t) \Gamma^+(t). \quad (6)$$

The factors of 0.5 in Eqs. (4) and (5) arise from the excess heat shown by Eqs. (B9) and (B10). These factors cancel

out in Eq. (6), resulting in the total heat \dot{Q}_T^{SS} being equal to the housekeeping heat $\dot{Q}_{\text{HK}}^{\text{SS}}$.

These equations give electronic and thermodynamic insights into the system in the non-equilibrium steady state. Since $e\Gamma^+(t)$ corresponds to electric current from the ER to the dot, Eq. (6) corresponds to the power dissipation to maintain the charge in the dot. From a thermodynamics viewpoint, Eq. (6) also represents the work rate on the ER-dot system.[35] Its time average is given by $2\gamma E_C \langle N_{\text{SS}} \rangle \bar{\Gamma}^+$, where γ monotonically decreases with an increase in βS_{AC} . Specifically, γ approximates 1 if $\beta e S_{\text{AC}} \gg 1$, and γ approximates 2 if $\beta e S_{\text{AC}} \ll 1$ [see Appendix E]. The assumption for this time average is that the phase ϕ of the AC signal is randomized. Eqs. (4) and (5) provide information about heat flow for maintaining the steady state. Eq. (4) represents heat dissipation when an electron with energy $-eV(t)$ in the ER enters the dot, whose effective chemical potential μ_{eff} is $2E_C \langle N_{\text{SS}} \rangle$, with transition rate $\bar{\Gamma}^+$. Here, the factors of 0.5 in these equations are ignorable because they originate from the excess heat. Eq. (5) represents heat dissipation when an electron in the dot returns to the ER whose Fermi energy E_{const} corresponds to that without the AC signal. Since the number of electrons entering and leaving the dot is the same in a steady state, the heat dissipation of $-eV(t)$ causes heat flow as described by Eqs. (4) and (5). This understanding is illustrated in Fig. 3(a).

Figure 3(b) shows \dot{Q}_T decomposition into \dot{Q}_{EX} and \dot{Q}_{HK} . At $t = 0$, \dot{Q}_{EX} is maximal. Then it decreases over time and becomes zero in the steady state, indicating the distance from the steady state. From Eqs. (B4) and (B5), $\dot{Q}_{\text{EX}} = \sum_{N=0}^{\langle N_{\text{SS}} \rangle} \beta^{-1} \ln(\rho_{N+1}^{\text{SS}}/\rho_N^{\text{SS}}) = E_C \langle N_{\text{SS}} \rangle^2$. This rightmost term represents the free energy ΔF_{SS} in the steady state, consistent with the experimental results.

On the other hand, \dot{Q}_{HK} gradually increases over time until the steady state, then approximates the constant value $\dot{Q}_{\text{HK}}^{\text{SS}}$ equal to $\dot{Q}_{\text{HK}}^{\text{SS}} = 2\gamma E_C \langle N_{\text{SS}} \rangle \bar{\Gamma}^+$. This increase in \dot{Q}_{HK} is because an increase in $\langle N(t) \rangle$ over time raises exit events from the dot, increasing the housekeeping-heat component in \dot{Q}^- in Eq. (5) [also see \dot{Q}_T decomposition into \dot{Q}^+ and \dot{Q}^- in Appendix C].

The experimental analysis on \dot{Q}_T and $\dot{Q}_{\text{HK}}^{\text{SS}}$, combined with the numerical analysis using the master equation of Eq.(1) provides insights into the free energy ΔF_{SS} in the steady state: $\int_0^{\tau_{\text{SS}}} \dot{Q}_T dt + \Delta F_{\text{SS}} = \int_0^{\tau_{\text{SS}}} \dot{Q}_{\text{HK}}^{\text{SS}} dt$, where τ_{SS} is the time interval until the ER-dot system reaches the non-equilibrium steady state. This correlation is denoted by the grey area between \dot{Q}_T and the constant $\dot{Q}_{\text{HK}}^{\text{SS}}$ shown in Fig. 3(b). For a qualitative explanation, we consider $\dot{Q}_{\text{HK}}^{\text{SS}}$ and μ_{eff} in the non-equilibrium steady state, shown by Fig. 3(a), as a reference. Until this steady state, since $\langle N(t) \rangle$ increases from zero to $\langle N_{\text{SS}} \rangle$, the number of electrons entering the dot exceeds those leaving by $\langle N_{\text{SS}} \rangle$. Consequently, $\int_0^{\tau_{\text{SS}}} \dot{Q}^- dt$

is smaller than $\int_0^{\tau_{\text{SS}}} \dot{Q}_{\text{HK}}^{\text{SS}} dt$ by $\langle N_{\text{SS}} \rangle \mu_{\text{eff}}$. Conversely, when an electron enters the dot, it dissipates heat, $Q_N^{+1} = [-eV(t) - \mu_{\text{eff}}] + (\mu_{\text{eff}} - \mu_{N+1})$, from Eq. (B2). The first term of the right-hand side corresponds to the housekeeping component, and the second corresponds to the additional or excess heat between μ_{eff} and μ_{N+1} . When an electron leaves and then re-enters the dot [an 'in-out event' in Fig. 3(a)], the net change in N is zero, and the additional heats cancel out. Instead, $-eV(t)$ remains as dissipation, as in the steady state. In other words, when the same number of electrons move in and out, they consume heat similarly to that in the steady state, whether before or after the steady state. Consequently, total heat dissipation $\int_0^{\tau_{\text{SS}}} \dot{Q}_T dt$ is smaller than $\int_0^{\tau_{\text{SS}}} \dot{Q}_{\text{HK}}^{\text{SS}} dt$ by $\langle N_{\text{SS}} \rangle \mu_{\text{eff}} - \sum_0^{\langle N_{\text{SS}} \rangle - 1} (\mu_{\text{eff}} - \mu_{N+1}) = E_C \langle N_{\text{SS}} \rangle^2 = \Delta F_{\text{SS}}$:

$$\int_0^{\tau_{\text{SS}}} \dot{Q}_T dt = \int_0^{\tau_{\text{SS}}} \dot{Q}_{\text{HK}}^{\text{SS}} dt - \Delta F_{\text{SS}}. \quad (7)$$

Using $\dot{Q}_T = \dot{Q}_{\text{EX}} + \dot{Q}_{\text{HK}}$, $\dot{Q}_{\text{EX}} = \Delta F_{\text{SS}}$, and Eq. (7) gives $\Delta F_{\text{SS}} = \frac{1}{2} \int_0^{\tau_{\text{SS}}} (\dot{Q}_{\text{HK}}^{\text{SS}} - \dot{Q}_{\text{HK}}) dt$. When $t \geq \tau_{\text{SS}}$, since $\dot{Q}_{\text{HK}} = \dot{Q}_{\text{HK}}^{\text{SS}} - \dot{Q}_{\text{HK}} = 0$, Eq. (7) always holds in the steady state.

Figure 3(a) provides a brief summary of heat dissipation rates or work-dissipation relation. Until a steady state, free energy is generated and \dot{Q}_{EX} is dissipated for an electron storage in the dot. When N increases by electron injection into the dot, $\dot{Q}^{+\text{SS}}$ and \dot{Q}_{EX} are dissipated with ΔF generation. When an electron leaves and enters the dot and the net N is zero, the heat corresponding to $\dot{Q}_{\text{EX}}^{\text{SS}}$ is dissipated. $\dot{Q}_{\text{EX}}^{\text{SS}}$ is decomposed into two types of heat dissipation, $(2\gamma E_C \langle N_{\text{SS}} \rangle - \mu_{\text{eff}})$ and $(\mu_{\text{eff}} - E_{\text{const}})$, for electron entering and leaving the dot, respectively. This heat dissipation is balanced with the work $2\gamma E_C \langle N_{\text{SS}} \rangle$. These insights help in understanding the efficiency discussed next.

These understandings based on Fig. 3(a) offer theoretical information on the efficiency for free-energy generation. We define the efficiency $\eta(t) = \Delta F(t)/[Q_T(t) + \Delta F(t)]$, where $Q_T(t) = \int_0^t \dot{Q}_T dt'$. The denominator corresponds to the work. Figure 4 shows the transient characteristics of $\eta(t)$ after applying the AC signal at different signal amplitudes S_{AC} : $\eta(t)$ rises, peaks, and then gradually decreases over time. Increasing S_{AC} raises the peak values of $\eta(t)$, in experiments, up to 0.25 at 150 mV.

To characterize $\eta(t)$, we consider the efficiency η_{SS} when the system reaches the non-equilibrium steady state at $t = \tau_{\text{SS}}$, since $\Delta F(t)$ reaches the maximum ΔF_{SS} given by $E_C \langle N_{\text{SS}} \rangle^2$ and $Q_T(t)$ after $t = \tau_{\text{SS}}$ is obtained from $(t - \tau_{\text{SS}}) \dot{Q}_{\text{HK}}^{\text{SS}}$. In a non-equilibrium steady state, Eq. (7) gives

$$\eta_{\text{SS}} = \frac{E_C \langle N_{\text{SS}} \rangle^2}{\int_0^{\tau_{\text{SS}}} \dot{Q}_{\text{HK}}^{\text{SS}} dt'}. \quad (8)$$

We define τ_{th} as the moment when $\langle N(t) \rangle$ reaches a

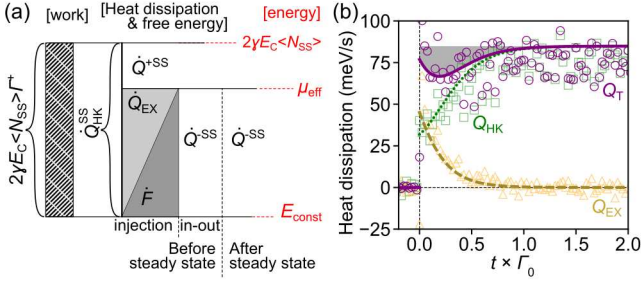


FIG. 3: (a) Schematic diagram of heat dissipation, free-energy generation, and work. The right and left vertical axes represent energy levels (written in red) and the rates of heat dissipation, free-energy generation, and work, respectively. The horizontal axis corresponds to events where electrons enter and leave the dot. "injection" and "in-out" events correspond to cases where N increases and where the same number of electrons enter and leave the dot, resulting in a net change in N being zero, both occurring before the steady state. Although these events occur randomly, events are categorized into two types for simplicity. The areas of the heat dissipation rates represent the total heat dissipation. (b) \dot{Q}_T and its decomposition into rates \dot{Q}_{EX} (dashed line, triangle scatter) and \dot{Q}_{HK} (dotted line, square scatter) of excess and housekeeping heats, respectively. The scatters are experimental results obtained from the average of 3000 repetitions. The lines represent values obtained from the master equation. The gray area represents $(\dot{Q}_{HK}^{SS} - \dot{Q}_T)$. S_{AC} was 100 mV.

threshold value of $a\langle N_{SS} \rangle$, where $0 < a < 1$. From Appendix D, τ_{th} is approximated as follows:

$$\tau_{th} \sim \frac{\langle N_{SS} \rangle}{\Gamma^+} \frac{4}{(\beta e S_{AC})^2} \ln \left(\frac{1}{1-a} \right) \text{ if } \beta e S_{AC} \ll 1, \quad (9)$$

$$\tau_{th} \sim \frac{\langle N_{SS} \rangle}{\Gamma^+} a \text{ if } \beta e S_{AC} \gg 1. \quad (10)$$

Eq. (9) indicates that smaller S_{AC} increases τ_{th} towards infinity. Eq. (10) implies that $\langle N(t) \rangle$ increases with the constant rate of Γ^+ over time. In both cases, τ_{SS} approximates to τ_{th} at $a \sim 1$. \dot{Q}_{HK}^{SS} is defined as $2\gamma E_C \langle N_{SS} \rangle \Gamma^+$ as explained above. Consequently, η_{SS} is given by

$$\eta_{SS} \sim -\frac{(\beta e S_{AC})^2}{16 \ln(1-a)} \text{ if } \beta e S_{AC} \ll 1, \text{ or} \quad (11)$$

$$\eta_{SS} \sim \frac{1}{a+1} = 0.5 \text{ if } \beta e S_{AC} \gg 1 \text{ and } a = 1. \quad (12)$$

These equations reveal some efficiency trends. When $S_{AC} \gg k_B T$, the efficiency approaches 0.5 near the non-equilibrium steady state. Larger S_{AC} drives the system far from initial equilibrium, unlike quasi-static operation for the Landauer limit. This high efficiency arises from shortened τ_{th} , reducing \dot{Q}^{-SS} before the steady state [see Fig. 3(a)]. Concurrently, reduced γ equalizes $2\gamma E_C \langle N_{SS} \rangle$ to μ_{eff} , reducing \dot{Q}^{+SS} . Sequentially, Q_T is dominated by Q_{EX} , while Q_{HK} remains negligible until the non-equilibrium steady state. Conversely, small S_{AC} increases

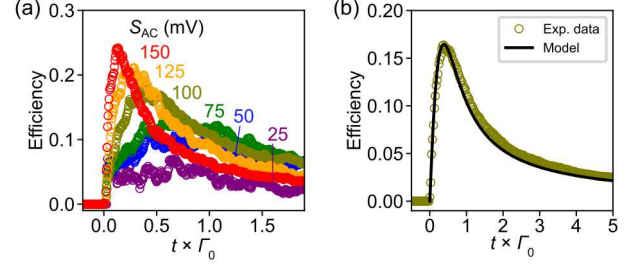


FIG. 4: Efficiency for free energy generation at different AC-signal amplitude S_{AC} . Each curve is averaged over 250 repetitions. Inset: comparison of the experimental results averaged over 30000 repetitions (open circles) at $S_{AC} = 100$ mV with the theoretical result (solid line) obtained from the master equation.

τ_{th} towards infinity, with γ approaching 2, leading to low efficiency.

Eqs. (11) and (12) are independent of E_C , which governs single-electron motion characteristics, such as $\langle N(t) \rangle$ and $\sigma^2(t)$, implying that single-electron motion itself is not important for device performance. It should be noted, however, that the single electron counting statistics play an important role in qualifying heat dissipation and free energy and then deriving and verifying the thermodynamics perspectives applicable to devices utilizing multiple electrons.

In summary, we demonstrated single-electron counting statistics for estimating the entropy production, heat decomposition, and free energy in a non-equilibrium small dot. These experimental results are explained mathematically using the master equation, revealing the correlation between heat dissipation and free energy. In addition to such thermodynamic information, its correlation with electronic parameters is also clarified. Since our device utilizes multiple electrons at room temperature, it opens the way to connect the thermodynamics to electronic devices for understanding their performance limits.

ACKNOWLEDGMENTS

The authors thank Yasuhiko Tokura in Tsukuba university for valuable support on the theory. They also thank Keiji Saito and Tan Van Vu in Kyoto university for fruitful discussion.

Appendix A: Device structure

Figure A1(a) shows the device structure fabricated from a silicon-on-insulator (SOI) wafer. The width and height of the SOI wire connected to a dot and ER was about 10 nm. The gate length of an LG made of polycrystalline silicon was about 10 nm. The width and height of the constriction part of the SOI channel of the sense-

FET functioning as a charge sensor was around 10 nm. An upper gate (UG) covering the whole area shown by the SEM image controls the current flowing through the sense-FET, and it induces electrons in the ER. A thickness of the buried SiO_2 was 400 nm.

Appendix B: Heat dissipated by one electron entering and leaving the dot

Heat dissipation is estimated from individual electron motions between the ER and dot. When the excess electron number in the dot changes from N to $N+1$ or $N-1$, its heat dissipation Q_N^{+1} or Q_N^{-1} , respectively, is given by

$$Q_N^{\pm 1} = H_{N\pm 1} - H_N. \quad (\text{B1})$$

Here, H_N is the Hamiltonian when the number of excess electrons in the dot is N : [33] $H_N = E_C(N - N_{\text{off}})^2 - E_C N_{\text{off}}^2$, where $N_{\text{off}} = -eV(t)/(2E_C)$. Consequently, Eq. (B1) yields [see Fig. 1(b)]

$$Q_N^{+1} = -eV(t) - \mu_{N+1}, \text{ and} \quad (\text{B2})$$

$$Q_N^{-1} = eV(t) + \mu_N. \quad (\text{B3})$$

These $Q_N^{\pm 1}$ can be decomposed into excess and housekeeping heats. [14] Excess heats $Q_{\text{EX},N}^{+1}$ and $Q_{\text{EX},N}^{-1}$ for an electron entering and leaving the dot when the excess electron number is N are given by

$$\beta Q_{\text{EX},N}^{\pm 1} = \ln \left(\frac{\rho_{N\pm 1}^{\text{SS}}}{\rho_N^{\text{SS}}} \right), \quad (\text{B4})$$

where ρ_N^{SS} is the steady-state probability distribution. ρ_N^{SS} follows a Gaussian distribution from the theoretical analysis based on the master equation and experimental results shown in Fig. 2(b), leading to

$$\rho_N^{\text{SS}} = Z^{-1} \exp[-\beta E_C (N - \langle N_{\text{SS}} \rangle)^2], \quad (\text{B5})$$

where $Z = \sum_{N=-\infty}^{\infty} \rho_N^{\text{SS}}$. Substituting Eq. (B5) into equation Eq. (B4) gives

$$Q_{\text{EX},N}^{+1} = 2E_C \langle N_{\text{SS}} \rangle - \mu_{N+1}, \text{ and} \quad (\text{B6})$$

$$Q_{\text{EX},N}^{-1} = -2E_C \langle N_{\text{SS}} \rangle + \mu_N. \quad (\text{B7})$$

Housekeeping heats $Q_{\text{HK},N}^{+1}$ and $Q_{\text{HK},N}^{-1}$ for an electron entering and leaving the dot, respectively, at N follow

$$\begin{aligned} \beta Q_{\text{HK},N}^{\pm 1} &= \ln \left[\frac{P(N \pm 1|N) \rho_N^{\text{SS}}}{P(N|N \pm 1) \rho_{N\pm 1}^{\text{SS}}} \right] \\ &= \pm [-eV(t) - 2E_{\text{AC}} \langle N_{\text{SS}} \rangle] \end{aligned} \quad (\text{B8})$$

Consequently, Eqs. (B2) and (B3) are decomposed:

$$\begin{aligned} Q_N^{+1} &= [-eV(t) - 2E_{\text{AC}} \langle N_{\text{SS}} \rangle \\ &\quad + [2E_{\text{AC}} \langle N_{\text{SS}} \rangle - \mu_{N+1}] \text{ and} \end{aligned} \quad (\text{B9})$$

$$\begin{aligned} Q_N^{-1} &= [eV(t) + 2E_{\text{AC}} \langle N_{\text{SS}} \rangle \\ &\quad + [-2E_{\text{AC}} \langle N_{\text{SS}} \rangle + \mu_N]. \end{aligned} \quad (\text{B10})$$

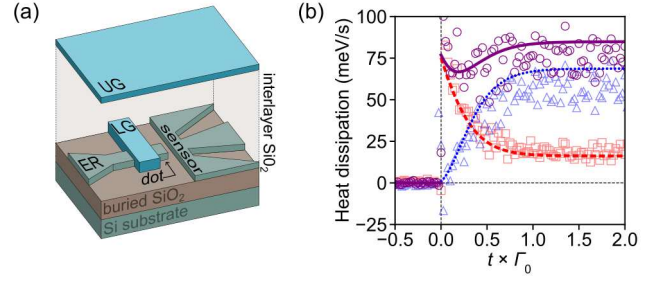


FIG. A1. (a) Schematic view of the device structure. Between the SOI layer and UG, there was an interlayer SiO_2 with a thickness of 80 nm. (b) Total dissipated heat rate \dot{Q}_T (full line, circle scatter) and its decomposition into rates \dot{Q}^+ (dashed line, square scatter) and \dot{Q}^- (dotted line, triangle scatter) for electrons entering and leaving the dot, respectively, during the state transition when the AC signal is applied at $t = 0$. The experimental plots depicted by open marks are obtained from the average of 3000 repetitions. The line plots represent theoretical values from the master equation.

The first and second square brackets on the right-hand sides correspond to housekeeping and excess heats, respectively.

Appendix C: Decomposition into \dot{Q}^+ and \dot{Q}^-

Figure A1(b) shows experimental and theoretical transient characteristics of \dot{Q}_T , \dot{Q}^+ , and \dot{Q}^- . At $t = 0$, \dot{Q}^+ is at its maximum value and \dot{Q}^- is zero, as $\langle N(0) \rangle$ is zero and $\rho_N(0)\Gamma_N^-$ is minimal [see Eqs. (2) and (3)]. Then, \dot{Q}^+ decreases and \dot{Q}^- increases because of an increase in $\langle N(t) \rangle$. Finally, \dot{Q}^+ and \dot{Q}^- asymptotically reach values given by the time-average forms of Eqs. (4) and (5) in a non-equilibrium steady state.

Appendix D: Approximation of Transient characteristics until a steady state

The transient characteristics of $\langle N(t) \rangle$ is given by [39]

$$\begin{aligned} \langle N(t) \rangle &= \frac{\langle N_{\text{SS}} \rangle}{\ln(\overline{\Gamma^+}/\Gamma_0)} \\ &\quad \times \ln \left[\frac{\overline{\Gamma^+}/\Gamma_0}{1 + (\overline{\Gamma^+}/\Gamma_0 - 1) \exp(-2\beta E_C \overline{\Gamma^+} t)} \right]. \end{aligned} \quad (\text{D1})$$

The moment τ_{th} when $\langle N(t) \rangle$ reaches a threshold value of $a\langle N_{\text{SS}} \rangle$, where $0 < a < 1$, is given by

$$\tau_{\text{th}} = \frac{\langle N_{\text{SS}} \rangle}{\Gamma^+} \frac{1}{\ln(\overline{\Gamma^+}/\Gamma_0)} \ln \left[\frac{\overline{\Gamma^+}/\Gamma_0 - 1}{(\overline{\Gamma^+}/\Gamma_0)^{1-a} - 1} \right]. \quad (\text{D2})$$

When $1/(1-a) \in \mathbb{N}$

$$\ln \left[\frac{\overline{\Gamma^+}/\Gamma_0 - 1}{(\overline{\Gamma^+}/\Gamma_0)^{1-a} - 1} \right] = \ln \left[\sum_{i=0}^{\frac{1}{1-a}-1} \left(\frac{\overline{\Gamma^+}}{\Gamma_0} \right)^{(1-a)i} \right]. \quad (\text{D3})$$

Using the integral formula of the modified Bessel functions,

$$\begin{aligned} \overline{\Gamma^+} &= \frac{\omega_{AC}}{2\pi} \int_0^{2\pi/\omega_{AC}} \Gamma_0 \exp[\beta e S_{AC} \sin(\omega_{AC} t)] dt \\ &= \Gamma_0 I_0(\beta e S_{AC}), \end{aligned} \quad (\text{D4})$$

where

$$I_0(x) = \sum_{s=0}^{\infty} \frac{1}{s!s!} \left(\frac{x}{2} \right)^{2s}. \quad (\text{D5})$$

When $\beta S_{AC} \ll 1$, Eq. (D4) is simplified to

$$\frac{\overline{\Gamma^+}}{\Gamma_0} \sim 1 + \frac{1}{4}(\beta e S_{AC})^2. \quad (\text{D6})$$

Using Eqs. (D3), (D6), and the Taylor expansion, Eqs. (D2) and (D1) can be converted to

$$\tau_{\text{th}} \sim \frac{\langle N_{\text{SS}} \rangle}{\overline{\Gamma^+}} \frac{4}{(\beta e S_{AC})^2} \ln \left(\frac{1}{1-a} \right) \quad \text{and} \quad (\text{D7})$$

$$\langle N(t) \rangle \sim \frac{\langle N_{\text{SS}} \rangle (\beta e S_{AC})^2}{4 \ln(\overline{\Gamma^+}/\Gamma_0)} [1 - \exp(-2\beta E_C \overline{\Gamma^+} t)], \quad (\text{D8})$$

respectively. Eq. (D8) represents the transient characteristics with a time constant of $(2\beta E_C \overline{\Gamma^+})^{-1}$.

When $\beta S_{AC} \gg 1$, the asymptotic form of the Bessel functions simplifies Eq. (D4) to

$$\begin{aligned} \frac{\overline{\Gamma^+}}{\Gamma_0} &= \frac{\exp(\beta e S_{AC})}{\sqrt{2\pi\beta e S_{AC}}} \left\{ 1 + \frac{1}{8\beta e S_{AC}} + \mathcal{O} \left[\frac{1}{(\beta S_{AC})^2} \right] \right\} \\ &\sim \frac{\exp(\beta e S_{AC})}{\sqrt{2\pi\beta e S_{AC}}}. \end{aligned} \quad (\text{D9})$$

Using Eqs. (D2), (D3), (D9) and $\ln(\overline{\Gamma^+}/\Gamma_0) \sim \beta e S_{AC}$,

$$\tau_{\text{th}} \sim \frac{\langle N_{\text{SS}} \rangle}{\overline{\Gamma^+}} a. \quad (\text{D10})$$

Appendix E: Approximation of housekeeping heat in a non-equilibrium steady state

Since $\dot{Q}_{\text{HK}}^{\text{SS}}$ is equal to $\dot{Q}_{\text{T}}^{\text{SS}}$, shown in Eq. (6), in a non-equilibrium steady state, its time-average can be given by

$$\begin{aligned} \dot{Q}_{\text{HK}}^{\text{SS}} &= -\frac{\omega_{AC}}{2\pi} \int_0^{2\pi/\omega_{AC}} e S_{AC} \sin(\omega_{AC} t) \\ &\quad \times \Gamma_0 \exp[-e S_{AC} \sin(\omega_{AC} t)] dt \\ &= \Gamma_0 e S_{AC} I_1(\beta e S_{AC}), \end{aligned} \quad (\text{E1})$$

where

$$I_1(x) = \sum_{s=0}^{\infty} \frac{1}{s!(s+1)!} \left(\frac{x}{2} \right)^{(2s+1)} \quad (\text{E2})$$

is the integral formula for the modified Bessel function. When $\beta e S_{AC} \ll 1$, Eqs. (D6) and the Taylor expansion approximates Eq. (E1):

$$\begin{aligned} \dot{Q}_{\text{HK}}^{\text{SS}} &\sim \Gamma_0 e S_{AC} \left[\frac{1}{2}(\beta e S_{AC}) + \frac{1}{16}(\beta e S_{AC})^3 \right] \\ &= \Gamma_0 \frac{(\beta e S_{AC})^2}{2\beta} \left[1 + \frac{1}{8}(\beta e S_{AC})^2 \right] \\ &\sim 4E_C \langle N_{\text{SS}} \rangle \overline{\Gamma^+} \end{aligned} \quad (\text{E3})$$

When $\beta e S_{AC} \gg 1$, the asymptotic form of the modified Bessel functions, Eq. (D9), and $\ln(\overline{\Gamma^+}/\Gamma_0) \sim \beta e S_{AC}$ simplify Eq. (E1) to

$$\dot{Q}_{\text{HK}}^{\text{SS}} \sim \Gamma_0 e S_{AC} \frac{\exp(\beta e S_{AC})}{\sqrt{2\pi\beta e S_{AC}}} \sim 2E_C \langle N_{\text{SS}} \rangle \overline{\Gamma^+}. \quad (\text{E4})$$

-
- [1] R. Landauer, Irreversibility and heat generation in the computing process, *IBM J. Res. Dev.* **5**, 183 (1961).
 [2] A. Bérut, A. Arakelyan, A. Petrosyan, S. Ciliberto, R. Dillenschneider, and E. Lutz, Experimental verification of landauer's principle linking information and thermodynamics, *Nature* **483**, 187 (2012).
 [3] Y. Jun, M. c. v. Gavrilov, and J. Bechhoefer, High-precision test of landauer's principle in a feedback trap, *Phys. Rev. Lett.* **113**, 190601 (2014).
 [4] J. V. Koski, V. F. Maisi, J. P. Pekola, and D. V. Averin, Experimental realization of a szilard engine with a single electron, *Proc. Natl. Acad. Sci. USA* **111**, 13786 (2014).
 [5] A. Bérut, A. Petrosyan, and S. Ciliberto, Information and thermodynamics: experimental verification of landauer's

- erasure principle, *J. Stat. Mech.* **2015**, P06015 (2015).
 [6] L. Martini, M. Pancaldi, M. Madami, P. Vavassori, G. Gubbiotti, S. Tacchi, F. Hartmann, M. Emmerling, S. Höfling, L. Worschech, and G. Carloti, Experimental and theoretical analysis of landauer erasure in nano-magnetic switches of different sizes, *Nano Energy* **19**, 108 (2016).
 [7] J. Hong, B. Lambson, S. Dhuey, and J. Bokor, Experimental test of landauer's principle in single-bit operations on nanomagnetic memory bits, *Science Advances* **2**, e1501492 (2016), <https://www.science.org/doi/pdf/10.1126/sciadv.1501492>.
 [8] D. Barker, M. Scandi, S. Lehmann, C. Thelander, K. A. Dick, M. Perarnau-Llobet, and V. F. Maisi, Experimental

- verification of the work fluctuation-dissipation relation, *Phys. Rev. Lett.* **128**, 040602 (2022).
- [9] N. Shiraishi, N. Saito, and H. Tasaki, Universal trade-off relation between power and efficiency for heat engines, *Phys. Rev. Lett.* **117**, 190601 (2016).
- [10] D. H. Wolpert, The stochastic thermodynamics of computation, *J. Phys. A* **52**, 193001 (2019).
- [11] K. Proesmans, J. Ehrich, and J. Bechhoefer, Finite-time landauer principle, *Phys. Rev. Lett.* **125**, 100602 (2020).
- [12] J. S. Lee, S. Y. Lee, H. Kwon, and H. Park, Speed limit for a highly irreversible process and tight finite-time landauer's bound, *Phys. Rev. Lett.* **129**, 120603 (2022).
- [13] Y. Oono and M. Paniconi, Steady state thermodynamics, *Prog. Theor. Phys. Supp.* **130**, 29 (1998).
- [14] T. Hatano and S. Sasa, Steady-state thermodynamics of langevin systems, *Phys Rev Lett* **86**, 3463 (2001).
- [15] M. Esposito, U. Harbola, and S. Mukamel, Entropy fluctuation theorems in driven open systems: Application to electron counting statistics, *Phys. Rev. E* **76**, 031132 (2007).
- [16] K. Yoshimura, A. Kolchinsky, A. Dechant, and S. Ito, Housekeeping and excess entropy production for general nonlinear dynamics, *Phys. Rev. Research* **5**, 013017 (2023).
- [17] U. Seifert, Entropy production along a stochastic trajectory and an integral fluctuation theorem, *Phys. Rev. Lett.* **95**, 040602 (2005).
- [18] P. Gaspard, Fluctuation theorem for nonequilibrium reactions, *The Journal of Chemical Physics* **120**, 8898 (2004).
- [19] T. Speck and U. Seifert, Integral fluctuation theorem for the housekeeping heat, *J. Phys. A: Math. Gen.* **38**, L581 (2005).
- [20] C. Van den Broeck and M. Esposito, Three faces of the second law. ii. fokker-planck formulation, *Phys. Rev. E* **82**, 011144 (2010).
- [21] M. Esposito and C. Van den Broeck, Three faces of the second law. i. master equation formulation, *Phys. Rev. E* **82**, 011143 (2010).
- [22] L. B. Kish, End of moore's law: thermal (noise) death of integration in micro and nano electronics, *Phys. Lett. A* **305**, 144 (2002).
- [23] A. S. Sadek, K. Nikolić, and M. Forshaw, Parallel information and computation with restitution for noise-tolerant nanoscale logic networks, *Nanotechnology* **15**, 192 (2003).
- [24] K. Palem, Energy aware computing through probabilistic switching: a study of limits, *IEEE Trans. Comput.* **54**, 1123 (2005).
- [25] T. J. Hamilton, S. Afshar, A. van Schaik, and J. Tapson, Stochastic electronics: A neuro-inspired design paradigm for integrated circuits, *Proceedings of the IEEE* **102**, 843 (2014).
- [26] K. Y. Camsari, R. Faria, B. M. Sutton, and S. Datta, Stochastic p-bits for invertible logic, *Phys. Rev. X* **7**, 031014 (2017).
- [27] J. Gu and P. Gaspard, Microreversibility, fluctuations, and nonlinear transport in transistors, *Phys. Rev. E* **99**, 012137 (2019).
- [28] N. Freitas, J. C. Delvenne, and M. Esposito, Stochastic thermodynamics of nonlinear electronic circuits: A realistic framework for computing around, *Phys. Rev. X* **11**, 10.1103/PhysRevX.11.031064 (2021).
- [29] N. Freitas, K. Proesmans, and M. Esposito, Reliability and entropy production in nonequilibrium electronic memories, *Phys. Rev. E* **105**, 034107 (2022).
- [30] D. V. Averin and J. P. Pekola, Statistics of the dissipated energy in driven single-electron transitions, *EPL (Europhysics Letters)* **96**, 67004 (2011).
- [31] B. Küng, C. Rössler, M. Beck, M. Marthaler, D. S. Golubev, Y. Utsumi, T. Ihn, and K. Ensslin, Irreversibility on the level of single-electron tunneling, *Phys. Rev. X* **2**, 011001 (2012).
- [32] O. P. Saira, Y. Yoon, T. Tanttu, M. Möttönen, D. V. Averin, and J. P. Pekola, Test of the jarzynski and crooks fluctuation relations in an electronic system, *Phys. Rev. Lett.* **109**, 180601 (2012).
- [33] J. P. Pekola and O. P. Saira, Work, free energy and dissipation in voltage driven single-electron transitions, *J. Low. Temp. Phys.* **169**, 70 (2012).
- [34] A. Hofmann, V. F. Maisi, C. Rössler, J. Basset, T. Krähenmann, P. Märki, T. Ihn, K. Ensslin, C. Reichl, and W. Wegscheider, Equilibrium free energy measurement of a confined electron driven out of equilibrium, *Phys. Rev. B* **93**, 035425 (2016).
- [35] A. Hofmann, V. F. Maisi, J. Basset, C. Reichl, W. Wegscheider, T. Ihn, K. Ensslin, and C. Jarzynski, Heat dissipation and fluctuations in a driven quantum dot, *Phys. Status. Solidi. B* **254**, 1600546 (2017).
- [36] P.-A. Carles, K. Nishiguchi, and A. Fujiwara, Deviation from the law of energy equipartition in a small dynamic-random-access memory, *Jpn. J. Appl. Phys.* **54**, 06FG03 (2015).
- [37] K. Nishiguchi, Y. Ono, and A. Fujiwara, Single-electron counting statistics of shot noise in nanowire si metal-oxide-semiconductor field-effect transistors, *Applied Physics Letters* **98**, 193502 (2011).
- [38] K. Nishiguchi, C. Koechlin, Y. Ono, A. Fujiwara, H. Inokawa, and H. Yamaguchi, Single-electron-resolution electrometer based on field-effect transistor, *Jpn. J. Appl. Phys.* **47**, 8305 (2008).
- [39] C. Sahlhani, K. Chida, T. Shimizu, T. Hayashi, and N. K., Alternating-current signal sensing beyond cutoff frequency using a single-electron dynamic random access memory, *Phys. Rev. Appl.* **to be published** (2025).
- [40] H. A. Kramers, Brownian motion in a field of force and the diffusion model of chemical reactions, *Physica* **7**, 284 (1940).
- [41] K. Nishiguchi, Y. Ono, and A. Fujiwara, Single-electron thermal noise, *Nanotechnology* **25**, 275201 (2014).
- [42] K. Chida, A. Fujiwara, and K. Nishiguchi, Noise-to-energy conversion in a nanometer-scale dot observed with electron counting statistics, *Appl. Phys. Lett.* **122**, 213502 (2023).
- [43] A. Andresen, Bjarne, R. S. Berry, A. Nitzan, and P. Salamon, Thermodynamics in finite time. i. the step-carnot cycle, *Phys. Rev. A* **15**, 2086 (1977).
- [44] V. Blickle and C. Bechinger, Realization of a micrometre-sized stochastic heat engine, *Nature Phys.* **8**, 143 (2012).
- [45] S. Carnot, Réflexions sur la puissance motrice du feu et sur les machines propres à développer cette puissance, *Annales scientifiques de l'École Normale Supérieure* **1**, 393 (1897).
- [46] S. Ciliberto, S. Joubaud, and A. Petrosyan, Fluctuations in out-of-equilibrium systems: from theory to experiment, *J. Stat. Mech-Theory E* **2010**, P12003 (2010).

- [47] D. Collin, C. Jarzynski, S. B. Smith, I. Tinoco, and C. Bustamante, Verification of the crooks fluctuation theorem and recovery of rna folding free energies, *nature* **437**, 231–234 (2005).
- [48] F. L. Curzon and B. Ahlborn, Efficiency of a carnot engine at maximum power output, *Am. J. Phys.* **43**, 22 (1975).
- [49] J. Gu and P. Gaspard, Stochastic approach and fluctuation theorem for charge transport in diodes, *Phys. Rev. E* **97**, 052138 (2018).
- [50] J. Hoppenau and A. Engel, On the work distribution in quasi-static processes, *J. Stat. Mech-Theory E* **2013**, P06004 (2013).
- [51] H. Hurwitz, Voltage fluctuations in a diode, *Phys. Rev.* **172**, 207 (1968).
- [52] J. V. Koski, V. F. Maisi, T. Sagawa, and J. P. Pekola, Experimental observation of the role of mutual information in the nonequilibrium dynamics of a maxwell demon, *Phys. Rev. Lett.* **113**, 030601 (2014).
- [53] I. A. Martínez, E. Roldán, L. Dinis, D. Petrov, J. M. R. Parrondo, and R. Rica, Brownian carnot engine, *Nature Phys.* **12**, 67 (2016).
- [54] A. Ryabov and V. Holubec, Maximum efficiency of steady-state heat engines at arbitrary power, *Phys. Rev. E* **93**, 050101 (2016).
- [55] T. Sagawa, Thermodynamics of information processing in small systems, *Prog Theor Phys* **127**, 1 (2012).
- [56] S. Toyabe, T. Sagawa, M. Ueda, E. Muneyuki, and M. Sano, Experimental demonstration of information-to-energy conversion and validation of the generalized jarzynski equality, *Nature Phys.* **6**, 988 (2010).
- [57] R.-X. Zhai, F.-M. Cui, Y.-H. Ma, C. P. Sun, and H. Dong, Experimental test of power-efficiency trade-off in a finite-time carnot cycle, *Phys. Rev. E* **107**, L042101 (2023).